45$^{th}$ Aerospace Sciences Meeting and Exhibit, January 8–11, 2007, Reno, Nevada

# Multi-point Aero-Structural Optimization of Wings Including Planform Variations

Antony Jameson*, Kasidit Leoviriyakit† and Sriram Shankaran
*Stanford Univerisity, Stanford, CA, 94305-4035, USA*

**This paper focuses on wing optimization via control theory using a multi-point design method. Based on the design methodology previously developed for wing section and planform optimization at a specific flight condition, it searches for a single wing shape that performs well over a range of flight conditions. Our previous experience with multi-point design without a detailed FE structural model, showed improvements in performance measures such as drag divergence Mach number and the lift-to-drag ratio over a range of Mach numbers. In the current work, the flow solution is modified to allow for shape deformation under load. We achieve this by coupling SYN107 to FEAP (Robert Taylor, University of California at Berkeley). The resulting aero-elastic simulation is then used to determine the optimal airfoil section and wing planform definition. In the multi-point design the actual shape will now be different at the different design points. With the coupled aero-structural analysis we hope to determine the best jig shape for the multi-point design.**

## I. Introduction

Aerodynamic shape optimization has become a standard practice today. It is widely accepted for optimizing the performance at one specific point. However, an important issue for single-point design is the performance penalty suffered by the same shape at other operating points. One way to seek a good compromise between multiple operating points is through multi-point optimization.

While multi-point design can be extended to most single-point design tools, the ultimate need is the development of an automated multi-point design tool. Here we formulate "automatic shape optimization via control theory" by combining computational fluid dynamics (CFD) with gradient-based optimization techniques, where the gradient is calculated based on the use of the control theory. For a wing design problem, the wing is treated as a device to control the flow to produce lift with minimum drag while satisfying a set of constraints governed by the flow equations and meeting other requirements such as low structural weight, sufficient fuel volume, and acceptable stability. This approach is radically different from conventional optimization methods. It treats the shape as a free surface and drives the flow solution, shape sensitivity, and final shape all to convergence simultaneously. Thus this approach is extremely efficient. During the last decade this method has been extensively developed to improve wing section shapes[1–5] and wing planforms.[6–11]

Our previous works[6–10] reported design methodology for wing planform optimization at a cruise condition. The main objective was to reduce drag of the airplane at constant lift, using the wing structural weight as a constraint to prevent un-realistic designs. Wing section and planform shapes were parameterized by mesh points and then used as the design variables. By allowing both section and planform variations, we could reduce both drag and structural weight of the airplane simultaneously while meeting other requirements such as lift, sufficient fuel volume, and stability constraints.

In this work, we report improvements in the wing design process by modifying the flow solution for shape deformation under load. We couple a freely available FE software, FEAP, with SYN107 to obtain the

*Thomas V. Jones Professor of Engineering, Department of Aeronautics and Astronautics, AIAA Member.
†AIAA Member

deflected shape of the wing. In multi-point design the actual shape will now be different at the different design points. Our aim is the find the best jig-shape for the multi-point design. This is important as from the first author's experience, the wing deflection can lead to twist variations of approximately 3 degrees at Mach 0.9, $CL = 0.5$.

## II. Mathematical formulation

### A. The control theory approach to wing design problems

The control theory approach has been proposed for shape design since 1974[12] but it did not have much impact on aerodynamic design until its application to transonic flow.[1] The major impact arose from its capability to effectively handle a design problem that involves a large number of design variables and is governed by a complex mathematical model, such as fluid flow. The control theory approach is often called the adjoint method since the necessary gradients are obtained through the solution of the adjoint equations of the governing equations.

In the context of control theory, a wing design problem can be considered as:

$$\begin{aligned} Minimizing \quad & I(w,S) \\ w.r.t \quad & S \\ subjected\ to \quad & R(w,S)=0 \end{aligned}$$

where $w$ is the flow variable, $S$ is the vector of wing design parameters, and $R(w,S)=0$ is the flow equation.

For instance, for a drag minimization problem we can take $I = C_D$ which is an integral of flow $w$ (pressure and shear force) over the wing $S$ (represented by parameters such as airfoils and planform). We modify $S$ (the airfoils and planform) to reduce the drag. The pressure and shear force are obtained from the flow equation $R = 0$ using CFD.

A change in $S$ results in a change

$$\delta I = \left[\frac{\partial I}{\partial w}\right]^T \delta w + \left[\frac{\partial I}{\partial S}\right]^T \delta S, \tag{1}$$

and $\delta w$ is determined from the equation

$$\delta R = \left[\frac{\partial R}{\partial w}\right] \delta w + \left[\frac{\partial R}{\partial S}\right] \delta S = 0. \tag{2}$$

The finite difference approach attempts to solve $\delta w$ from equation (2) and substitute it into equation (1) to calculate $\delta I$. For a design problem of $n$ design parameters e.g. $\mathcal{O}(S) = n$, this procedure requires a well-converged solution of $n + 1$ flow analysis problems to obtain the design sensitivities. Thus it becomes impractical when $n$ becomes large.

For an adjoint approach, we try to avoid solving for $\delta w$. This is done by introducing a Lagrange multiplier $\psi$, and subtracting the variation $\delta R$ from the variation $\delta I$ without changing the result. Thus, equation (1) can be replaced by

$$\begin{aligned} \delta I &= \left[\frac{\partial I}{\partial w}\right]^T \delta w + \left[\frac{\partial I}{\partial S}\right]^T \delta S - \psi^T \left( \left[\frac{\partial R}{\partial w}\right] \delta w + \left[\frac{\partial R}{\partial S}\right] \delta S \right) \\ &= \left\{ \left[\frac{\partial I}{\partial w}\right]^T - \psi^T \left[\frac{\partial R}{\partial w}\right] \right\} \delta w + \left\{ \left[\frac{\partial I}{\partial S}\right]^T - \psi^T \left[\frac{\partial R}{\partial S}\right] \right\} \delta S \end{aligned} \tag{3}$$

Choosing $\psi$ to satisfy the adjoint equation,

$$\left[\frac{\partial R}{\partial w}\right]^T \psi = \left[\frac{\partial I}{\partial w}\right], \tag{4}$$

the first term is eliminated, and we find that

$$\delta I = \mathcal{G}^T \delta S, \tag{5}$$

where

$$\mathcal{G}^T = \left[\frac{\partial I}{\partial S}\right]^T - \psi^T \left[\frac{\partial R}{\partial S}\right].$$

The advantage is that equation (5) is independent of $\delta w$, with the result that the gradient of $I$ with respect to an arbitrary number of design variables can be determined without the need for additional flow-field evaluations.

Once the gradient vector $\mathcal{G}$ has been established, it may now be used to determine a direction of improvement. The simplest procedure is to make a step in the negative gradient direction (steepest descent method) by setting

$$\delta S = -\lambda \mathcal{G}$$

where $\lambda$ is positive and small enough that the first variation is an accurate estimate of $\delta I$. The variation of the cost function then becomes

$$\begin{aligned} \delta I &= -\lambda \mathcal{G}^T \mathcal{G} \\ &\leq 0 \end{aligned}$$

More sophisticated search procedures may be used such as quasi-Newton methods, which attempt to estimate the second derivative $\frac{\partial^2 I}{\partial S_i \partial S_j}$ of the cost function from changes in the gradient $\frac{\partial I}{\partial S}$ in successive optimization steps. These methods also generally introduce line searches to find the minimum in the search direction which is defined at each step. Reference[13] provides a good description for those techniques. However, not all the techniques are practical for our wing design problem. Line searches, for example, would require extra flow calculations, which we try to avoid.

### B. Design using the Navier-Stokes equations

In this section we illustrate the application of control theory to aerodynamic design problems, using the three-dimensional compressible Navier-Stokes equations as a mathematical model. For convenience, let $\xi_1$, $\xi_2$, and $\xi_3$ denote the transformed coordinates and a repeated index $i$ imply a summation over $i = 1$ to 3. Then, in a fixed computational domain the flow equation $R(w, S) = 0$ takes the form

$$\frac{\partial (Jw)}{\partial t} + \frac{\partial (F_i - F_{vi})}{\partial \xi_i} = 0 \quad \text{in } \mathcal{D}, \tag{6}$$

where $J$ is the cell volume, $F_i$ and $F_{vi}$ are the inviscid and viscous terms which have the form

$$F_i = S_{ij} f_j \quad \text{and} \quad F_{vi} = S_{ij} f_{vj}.$$

Here $S_{ij}$ is the coefficient of the Jacobian matrix of the transformation which represents the projection of the $\xi_i$ cell face along the Cartesian $x_j$ axis. Moreover, because the computational boundary usually aligns with the body surface, $S_{ij}$ on the boundary also represents the geometry we are redesigning.

Suppose we want to minimize the cost function of a boundary integral

$$I = \int_{\mathcal{B}} \mathcal{M}(w, S)\, d\mathcal{B}_\xi \tag{7}$$

where the integral of $\mathcal{M}(w, S)$ could be a pure aerodynamic cost function such drag coefficient, or a multi-disciplinary cost function such as combination of drag and structural weight which is shown to be necessary for a planform design problem in references.[6–10]

In the steady flow the transient term of equation (6) drops out and the the adjoint problem can be formulated by combining the variations of equations (7) and (6) using the Lagrange multiplier $\psi$ as

$$\delta I = \int_{\mathcal{B}} \delta \mathcal{M}(w, S)\, d\mathcal{B}_\xi - \int_{\mathcal{D}} \psi^T \frac{\partial}{\partial \xi_i} \delta (F_i - F_{vi})\, d\mathcal{D}_\xi$$

If $\psi$ is differentiable, the second term on the right hand side can be integrated by parts, resulting

$$\delta I = \int_{\mathcal{B}} \delta \mathcal{M}(w, S)\, d\mathcal{B}_\xi - \int_{\mathcal{B}} n_i \psi^T \delta (F_i - F_{vi})\, d\mathcal{B}_\xi + \int_{\mathcal{D}} \frac{\partial \psi^T}{\partial \xi_i} \delta (F_i - F_{vi})\, d\mathcal{D}_\xi \tag{8}$$

The terms $\delta\mathcal{M}$, $\delta F_i$, and $\delta F_{vi}$ can be split into contributions associated with $\delta w$ and $\delta S$ using the subscript $I$ and $II$ to distinguish the variation of the flow solution and those associated with the metric variations as

$$\delta\mathcal{M} = [\mathcal{M}_w]_I\,\delta w + \delta\mathcal{M}_{II}, \quad \delta F_i = [F_{iw}]_I\,\delta w + \delta F_{iII}, \text{ and } \quad \delta F_{vi} = [F_{viw}]_I\,\delta w + \delta F_{viII}.$$

By collecting all the terms that multiply $\delta w$ of equation (8), the adjoint equation can be formulated. However since the velocity derivatives $\frac{\partial u_i}{\partial x_j}$ in the viscous flux are not explicitly expressed in terms of the state variable $w$, it is more convenient to introduce the transformation to the primitive variable $\tilde{w}^T = (\rho, u_1, u_2, u_3, p)$, and the relations $\delta w = M\delta\tilde{w}$. This yields the adjoint equations for the Navier-Stokes equation as

$$\left[S_{ij}\frac{\partial f_j}{\partial w}\right]^T \frac{\partial\psi}{\partial\xi_i} - M^{-1^T}\tilde{L}\psi = 0 \quad \text{in } \mathcal{D} \tag{9}$$

where

$$\begin{aligned}
(\tilde{L}\psi)_1 &= -\tfrac{p}{\rho^2}\tfrac{\partial}{\partial\xi_l}\left(S_{lj}\kappa\tfrac{\partial\theta}{\partial x_j}\right)\\
(\tilde{L}\psi)_{i+1} &= \tfrac{\partial}{\partial\xi_l}\left\{S_{lj}\left[\mu\left(\tfrac{\partial\phi_i}{\partial x_j}+\tfrac{\partial\phi_j}{\partial x_i}\right)+\lambda\delta_{ij}\tfrac{\partial\phi_k}{\partial x_k}\right]\right\}\\
&+ \tfrac{\partial}{\partial\xi_l}\left\{S_{lj}\left[\mu\left(u_i\tfrac{\partial\theta}{\partial x_j}+u_j\tfrac{\partial\theta}{\partial x_i}\right)+\lambda\delta_{ij}u_k\tfrac{\partial\theta}{\partial x_k}\right]\right\}\\
&- \sigma_{ij}S_{lj}\tfrac{\partial\theta}{\partial\xi_l} \qquad\qquad \text{for} \quad i=1,2,3\\
(\tilde{L}\psi)_5 &= \tfrac{1}{\rho}\tfrac{\partial}{\partial\xi_l}\left(S_{lj}\kappa\tfrac{\partial\theta}{\partial x_j}\right),
\end{aligned}$$

using $\psi_{j+1} = \phi_j$ for $j = 1, 2, 3$ and $\psi_5 = \theta$.

The form of the adjoint boundary conditions depends on the cost function. Table 1 summarizes some of the commonly used cost functions.

**Table 1. Adjoint boundary conditions for various cost functions**

| Category | $I$ | Adjoint boundary conditions |
|---|---|---|
| Drag minimization | $C_D = \int_{\mathcal{B}} q_i\tau_i dS$ | $\phi_k = q_k$ |
| Weight minimization | $C_W = \frac{-\beta}{cos(\Lambda)^2}\oint_{\mathcal{B}} p(\xi_1,\xi_3)K(\xi_3)S_{22}d\xi_1 d\xi_3$ | $\psi_{j+1}n_j = \frac{-\beta}{cos(\Lambda)^2}K\frac{S_{22}}{\lvert S_2\rvert}$ |
| Inverse design | $\frac{1}{2}\int_{\mathcal{B}}(p-p_d)^2\,dS$ | $\psi_{j+1}n_j = p - p_d$ |

The remaining terms from equation (8) then yield a simplified expression for the variation of the cost function which defines the gradient

$$\delta I = \int_{\mathcal{B}}\left\{\delta\mathcal{M}_{II} - n_i\psi^T\left[\delta F_i - \delta F_{vi}\right]_{II}\right\}d\mathcal{B}_\xi + \int_{\mathcal{D}}\left\{\frac{\partial\psi^T}{\partial\xi_i}\left[\delta F_i - \delta F_{vi}\right]_{II}\right\}d\mathcal{D}_\xi.$$

This equation can be further simplified by integrating the last term by parts, resulting in

$$\delta I = \int_{\mathcal{B}}\delta\mathcal{M}_{II}d\mathcal{B}_\xi - \int_{\mathcal{D}}\psi^T\frac{\partial}{\partial\xi_i}\delta(F_i - F_{vi})_{II}d\mathcal{D}_\xi. \tag{10}$$

This simplification turns out to be crucial for planform gradient calculations.

Once this gradient is evaluated, we can follow the design process outlined in section A to get an optimum shape. In addition, based on the fact that the gradient $\mathcal{G}$ is generally of a lower smoothness class than the shape $S$, it is important to restore the smoothness.[14] This may be affected by passing to a Sobolev inner product of the form

$$\langle u, v\rangle = \int (uv + \epsilon\frac{\partial u}{\partial\xi}\frac{\partial v}{\partial\xi})\,d\xi$$

This is equivalent to replacing $\mathcal{G}$ by $\bar{\mathcal{G}}$, where in one dimension

$$\bar{\mathcal{G}} - \frac{\partial}{\partial\xi}\epsilon\frac{\partial\bar{\mathcal{G}}}{\partial\xi} = \mathcal{G}, \quad \bar{\mathcal{G}} = \text{zero at end points}$$

and making a shape change $\delta S = -\lambda\bar{\mathcal{G}}$. Then for small positive $\lambda$

$$\delta I \;=\; -\lambda\langle\bar{\mathcal{G}},\bar{\mathcal{G}}\rangle \;\leq\; 0$$

guaranteeing an improvement.

# III. Implementation

Since a multi-point design is essentially an extension of a single-point design to perform at multiple design conditions, we first review the design methodology of a single-point design for wing section and planform. Then we describe the techniques to combine multiple results together.

## A. Single-point planform optimization

During the last decade, research on section optimization for a fixed wing planform have verified that the adjoint method has been perfected for transonic wing design. The process produces a shock free wing very rapidly.

However for the purpose of drag minimization, shock drag is not the only contribution to drag. Table 2 shows a breakdown of the drag for a typical long-range transport aircraft. Clearly, the major contribution

**Table 2. Typical drag breakdown of transport aircraft at cruise condition (1 count = 0.0001)**

| Item | $C_D$ | Cumulative $C_D$ |
|---|---|---|
| Wing pressure | 120 counts | 120 counts |
| | (15 shock,105 induced) | |
| Wing friction | 45 | 165 |
| Fuselage | 50 | 215 |
| Tail | 20 | 235 |
| Nacelles | 20 | 255 |
| Other | 15 | 270 |
| | — | |
| Total | 270 | |

comes from the induced drag (roughly 45 % of the total drag). It is well known that changes in the wing planform such as span, chord distribution, and taper directly affect the induced drag. Moreover, the sweep and section thickness also affect the shock drag. Thus planform optimization has potential to yield large improvement. However these changes also affect the structural weight of the wing. Therefore it is necessary to take into account both the aerodynamics and structural weight. Then the cost function becomes a combination of aerodynamics and structure weight.

### 1. *Cost function and design parameters*

Following our previous works,[6–11] we redesign both wing section and planform to minimize the cost function

$$I = \alpha_1 C_D + \alpha_2 \frac{1}{2} \int_{\mathcal{B}} (p - p_d)^2 dS + \alpha_3 C_W, \qquad (11)$$

The wing section is modeled by surface mesh points and the wing planform is simply modeled by the design variables shown in figure 1 as root chord ($c_1$), mid-span chord ($c_2$), tip chord ($c_3$), span ($b$), sweepback($\Lambda$), and wing thickness ratio ($t$). This choice of design parameters will lead to an optimum wing shape that will not require an extensive structural analysis and can be manufactured effectively. In the industry standard, it may require upto three hundred parameters to completely describe the wing planform. Although we demonstrate our design methodology using the simplified planform, our design method is still applicable to the industry standard because the adjoint method is independent of the number of design variables. Thus our method can be easily extend to cover many parameters without an increase in computational cost.

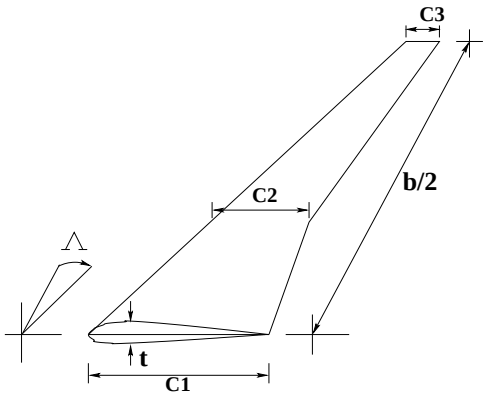


**Figure 1. Simplified wing planform of a transport aircraft.**

Notice further that this choice of design parameter allows the variation of the wing area. To avoid confusion, all the non-dimensional parameters in the cost function ($C_D$, $C_L$, and $C_W$) are normalized by fixed reference area $S_{ref}$.

### 2. *Structural model*

The wing structure was modeled in our earlier study by a box beam shown in figure2, whose major structural material is the box skin. The skin thickness ($t_s$) varies along the span and resists the bending moment caused by the wing lift. Then, the structural wing weight can be calculated based on material of the skin as

$$W_{wing} = \rho_{mat} g \int_{structual\ span} 2 t_s c_s dl$$

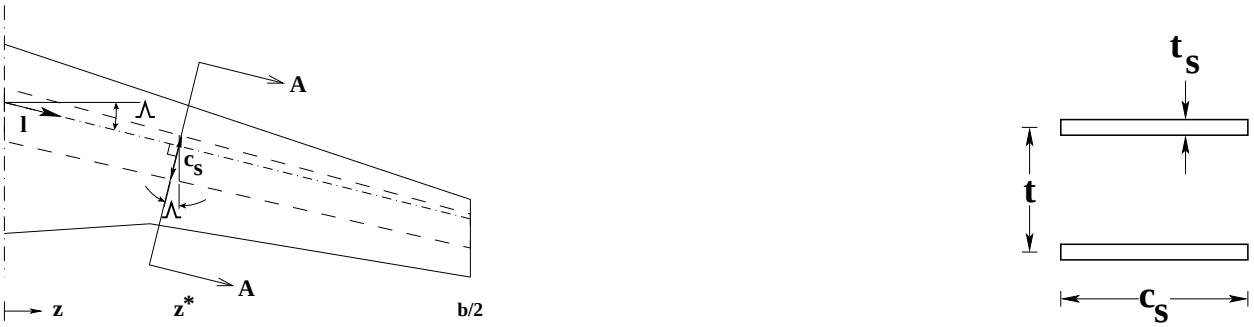


(a) swept wing planform

(b) section A-A

**Figure 2. Structural model for a swept wing**

In this work, we provide a more detailed model for the structural layout of the wing. In particular the wing is now modeled using a combination of skin, ribs and spar elements. These are modeled as shell elements and the wing weight is now computed as the

$$W_{wing} = \rho_{mat} g \int_V dl\ db\ dt$$

where $dl, db$ and $dt$ correspond to the length, breadth and thickness dimensions of the structural elements.

### 3. *Choice of the weighting constants*

In equation (11) the coefficient $\alpha_2$ is introduced to provide the designer some control over the pressure distribution, while the relative importance of drag and weight are represented by the coefficients $\alpha_1$ and $\alpha_3$. By varying these constants it is possible to calculate the Pareto front[16] of designs which have the least weight for a given drag coefficient, or the least drag coefficient for a given weight. The relative importance of these constants can be estimated from the Breguet range equation[a];

$$\begin{aligned} \frac{\delta R}{R} &= -\left( \frac{\delta C_D}{C_D} + \frac{1}{log\frac{W_1}{W_2}} \frac{\delta W_2}{W_2} \right) \\ &= -\left( \frac{\delta C_D}{C_D} + \frac{1}{log\frac{W_1}{W_2}} \frac{\delta C_W}{\frac{W_2}{q_\infty S_{ref}}} \right). \end{aligned}$$

The range of the aircraft is maximized when

$$\frac{\alpha_3}{\alpha_1} = \frac{C_D}{C_{W_2} log\frac{C_{W_1}}{C_{W_2}}}. \tag{12}$$

[a] $$R = \frac{V}{sfc} \frac{L}{D} log\frac{W_0 + W_f}{W_0}$$
where $V$ is the speed, $\frac{L}{D}$ is the lift-to-drag ratio, $sfc$ is the specific fuel consumption of the engines, $W_0$ is the landing weight, and $W_f$ is the weight of the fuel burnt.

### B. Multi-point planform optimization

Since airplanes operate at many different flight conditions from take-off to landing, it is important to account both design and off-design conditions during the optimization.

Let $I_j$ be the cost function at flight condition $j$ where $j = 1, 2, \ldots, n$ for $n$ flight conditions. Moreover let $I_j$ follow the form defined by equation (11). Then the total cost function becomes

$$I = \beta_1 I_1 + \beta_2 I_2 + \ldots + \beta_n I_n, \tag{13}$$

using

$$\beta_1 + \beta_2 + \ldots + \beta_n = 1$$

Choice of $\beta$ depends on the importance of the flight condition and may be defined based on the experience of the designer.

Then the gradient can be calculated by weighted average from a different design case as

$$g = \beta_1 g_1 + \beta_2 g_2 + \ldots + \beta_n g_n, \tag{14}$$

and the design process can be expressed as in figure 3.

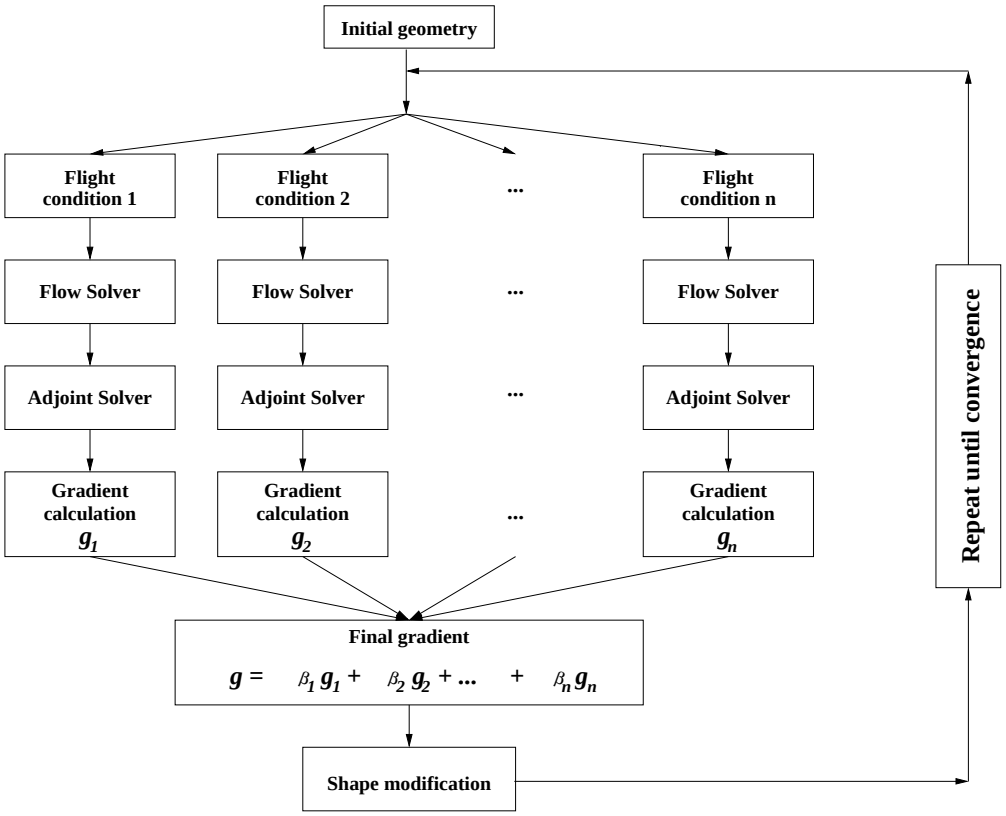


**Figure 3. Multi-point design process.**

Once the gradients are estimated, the shape change is then applied to the current jig-shape to determine the undeformed shape used by the aero-structural analysis.

## IV. Results

In this section, we present results from a multi-point design that includes a detailed FE analysis to determine the structural deflections. The main goal of any multi-point design is to find a single shape that performs well, over a range of conditions. Because a long range transport aircraft spends most time at the cruise condition, more emphases should be placed on cruise performance.

Our approach in this work is to use multi-point design to relieve undesired characteristics emerging from the cruise-optimized shape at the off-design conditions. From the baseline wing, we start by optimizing wing sections and planform at the cruise condition. The results are presented in the following sections.

### A. Single-point wing section and planform optimization

Here, we choose the Boeing 747 wing fuselage combination at the cruise condition Mach .87 and a lift coefficient $C_L = 0.45$ as a baseline configuration. The computational mesh is shown in figure 4. On this 256x64x48 grid, the wing sections are represented by 4224 surface mesh points and six planform variables (sweepback, span, chords at three span stations, and wing thickness) are extracted from these mesh points.

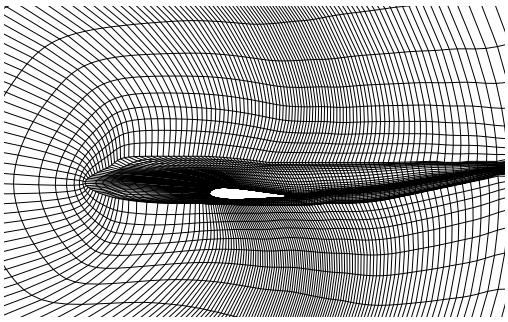

**Figure 4. Computational Grid of the B747 Wing Fuselage. Mesh size 256x64x48.**

Aero-elastic simulations are used to predict the deflected shape of the wing by coupling the flow solver with FEAP. Typically, three iterations during the first design cycle are required to obtain a converged deflected shape. 50 iterations of the multi-grid driven flow solver were used in the aero-elastic simulation. The wing was modeled with 129x33 skin elements (0.25 inches thick), 33 spar elements (1.0 inches thick) for the front and rear spar and 129 elements for each of the 33 ribs (0.5 inches thick) (shown in figure 5). All elements were modeled as shell elements with 6 degrees of freedom in FEAP. The aero-elastic simulations were assumed to have converged when the RMS value of the displacements fell below 1 mm. Figure 6 shows the original (blue) and deflected (red) shape of the wing as seen from mid-fuselage.

We allow simultaneous variations of the sections and planform to optimize the cost function defined in equation (11). We set $\alpha_2 = 0$ and the ratio $\alpha_3/\alpha_1$ according to equation (12) to maximize the range. After 50 design cycles (total computational cost of flow and gradient calculation is equivalent to 12 flow solutions), improvement in both drag and structural weight can be achieved. Table 3 shows this improvement.

**Table 3. Redesign of Boeing 747 at Mach .87 and $C_L$.45using the Reynolds Averaged Navier-Stokes equations with Baldwin-Lomax turbulent model.**

| Configuration | $C_D$ (counts) | $C_W$ (counts) |
|---|---|---|
| Boeing 747 | 135.8 | 508 |
| Redesign | 114 | 409 |

Figure 7 shows the changes in the wing planform. The optimum wing has a larger span, a lower sweep angle, and thicker wing sections. The increase in span leads to a reduction in the induced drag, while the section shape changes keep the shock drag low. At the same time the lower sweep angle and thicker wing section reduce the structural weight. Overall, the optimum wing improves both aerodynamic performance and structural weight (figures 8, 9).

Our previous attempts at estimating the trade-off between aerodynamic and structural performance used a simplified structural model. The trends predicted by our current method that uses a higher-fidelity structural model are similar to those obtained with a simplified structural model. Both optimization exercises result in a wing with slightly larger span, reduced LE sweep and thicker sections. The actual estimate of $C_D$ and $C_W$ are different, as expected, and the final angle attack required to maintain the prescribed lift is higher by about 0.5 degrees for the optimization that uses a detailed FE model.

### B. Multi-point redesign of the Boeing 747 wing

In this section, we repeat the optimization procedure for a two-point design, using the condition in table 4. Both flight conditions are equally weighted and 50 design cycles were used to determine the optimal wing shape. 50 multigrid cycles were used for the flow and the adjoint solution within each design cycle and as

in the single-point design calculations viscous meshes with dimensions of 256x64x48 were used. Aeroelastic simulations were assumed to have converged when the RMS of the deflections were below 1 mm. The shape changes were estimated from the accumulated gradient for the baseline configuration as in the multi-point case, the deflected wing shapes could be different.

**Table 4. Flight condition for two-point design**

| Condition | Mach | Target $C_L$ | $\beta$ |
|---|---|---|---|
| 1 | 0.85 | .45 | $\frac{1}{2}$ |
| 2 | 0.87 | .45 | $\frac{1}{2}$ |

Table 5 shows the result of the multi-point optimization. Interestingly, the improvement in aerodynamic and structural performance is substantially reduced when the optimization procedure was used in a multi-point setting. A closer look at the traversal of the design space suggests that during the intial stages of the optimization, the gradient with respect to span has opposite signs and hence the direction for improvement for one design point results in a deterioration for the other. However, the final wing shape has the same trend as in the single-point design case, lower LE sweep, slightly larger span and thicker airfoils, resulting is weaker shocks and structural weight.

**Table 5. Results of the Optimization for two-point design**

| Condition | Mach | Target $C_L$ | $\beta$ | $C_{D_i}$ | $C_{W_i}$ | $C_{D_f}$ | $C_{W_f}$ |
|---|---|---|---|---|---|---|---|
| 1 | 0.85 | .45 | $\frac{1}{2}$ | 121.0 | 540 | 116.7 | 532 |
| 2 | 0.87 | .45 | $\frac{1}{2}$ | 135.8 | 508 | 134.7 | 504 |

To establish confidence in the choice of optimization parameters and the stability of the optimum recovered by the design process, we repeated the design procedure on another wing-body configuration of interest and observed similar behavior, substantially reduced improvements in performance over the single-point design, competing nature of the different points in the optimization resulting in wings with lower LE sweep, slightly larger span and thicker airfoil sections.

However, repeating these optimization procedures with differing structural models resulted in significantly different optimum wing shapes. For example, doubling the thickness of the skins resulted in a change in the sign of the gradient with respect to the span variable for one of the design points thereby altering the progression of the design iterates.

## V. Conclusion

The inclusion of a detailed FE analysis within an aero-structural optimization procedure does not alter the trends from a simplified box-beam structural model. However, the estimates of the aerodynamic and structurasl performance are different and probably more accurate. For multi-point optimizations, the improvement in aerodynamic and structural performance are not as substantial as in the single-point case. It is not immediately clear whether this is an artifact of the design point chosen in this study.

## VI. Acknowledgment

This work has benefited greatly from the support of the Air Force Office of Science Research under grant No. AF F49620-98-1-2005.

## References

[1]A. Jameson. Aerodynamic design via control theory. *Journal of Scientific Computing*, 3:233–260, 1988.
[2]A. Jameson. Computational aerodynamics for aircraft design. *Science*, 245:361–371, 1989.

[3]A. Jameson, L. Martinelli, and N. A. Pierce. Optimum aerodynamic design using the Navier-Stokes equations. *Theoretical and Computational Fluid Dynamics*, 10:213–237, 1998.

[4]A. Jameson, J. J. Alonso, J. Reuther, L. Martinelli, and J. C. Vassberg. Aerodynamic shape optimization techniques based on control theory. *AIAA paper 98-2538*, AIAA 29th Fluid Dynamics Conference, Albuquerque, NM, June 1998.

[5]J. R. R. A. Martins. *A Coupled-Adjoint Method for High-Fidelity Aero-Strucural Optimization. PhD Dissertation*, Stanford University, Stanford, CA, October 2002.

[6]K. Leoviriyakit and A. Jameson. Aerodynamic shape optimization of wings including planform variables. *AIAA paper 2003-0210*, 41st Aerospace Sciences Meeting & Exhibit, Reno, Nevada, January 2003.

[7]K. Leoviriyakit, S. Kim, and A. Jameson. Viscous aerodynamic shape optimization of wings including planform variables. *AIAA paper 2003-3498*, 21st Applied Aerodynamics Conference, Orlando, Florida, June 2003.

[8]K. Leoviriyakit and A. Jameson. Aero-structural wing planform optimization. *AIAA paper 2004-0029*, 42nd Aerospace Sciences Meeting & Exhibit, Reno, Nevada, January 2004.

[9]K. Leoviriyakit and A. Jameson. Case studies in aero-structural wing planform and section optimization. *AIAA paper 2004-5372*, $22^{nd}$ Applied Aerodynamics Conference and Exhibit, Providence, Rhode Island, August 16-19, 2004 2004.

[10]K. Leoviriyakit, S. Kim, and A. Jameson. Aero-structural wing planform optimization using the Navier-Stokes equations. *AIAA paper 2004-4479*, 10th AIAA/ISSMO Multidisciplinary Analysis and Optimization Conference, Albany, New York, August 30 - September 1 2004.

[11]K. Leoviriyakit. *Wing Optimization via an Adjoint Method. PhD Dissertation*, Stanford University, Stanford, CA, December 2004.

[12]O. Pironneau. *Optimal Shape Design for Elliptic Systems*. Springer-Verlag, New York, 1984.

[13]P.E. Gill, W. Murray, and M.H. Weight. *Practical Optimization*. Academic Press, 111 Fifth Avenue, New York, New York 10003, 1981.

[14]A. Jameson and J. C. Vassberg. Studies of alternative numerical optimization methods applied to the brachistochrone problem. *Computational Fluid Dynamics Journal*, 9:281–296, 2000.

[15]Ilan Kroo. Aircraft design: Synthesis and analysis. http://adg.stanford.edu/aa241/AircraftDesign.html, January 2003. Section 10. Structure and weights.

[16]K. Deb. *Multi-Objective Optimization using Evolutionary Algorithms*. John Wiley & Sons, LTD, England, 2002.

[17]C. S. Morawetz. On the non-existence of continuous transonic flows past profiles. *Comm. Pure. Appl. Math.*, 9:45–48, 1956.

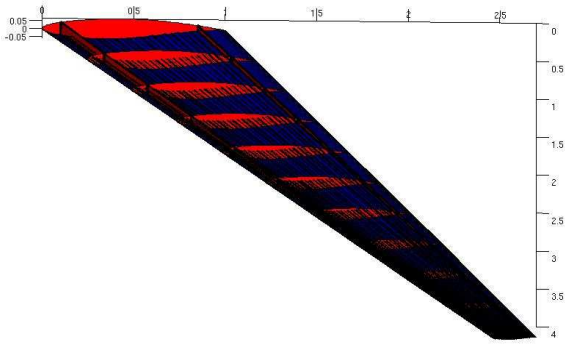


**Figure 5. Cut-away of the structural model for the wing, showing skin, ribs, spars and stiffeners**

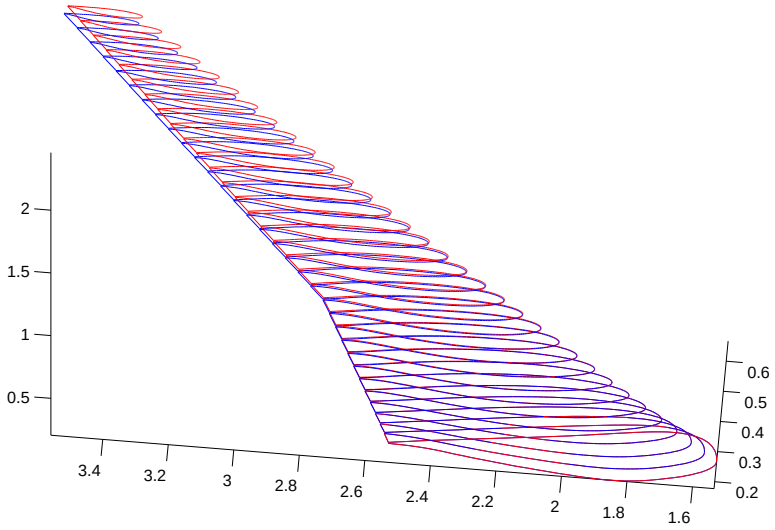


**Figure 6. Original (blue) and deflected (red) shape of the wing.**

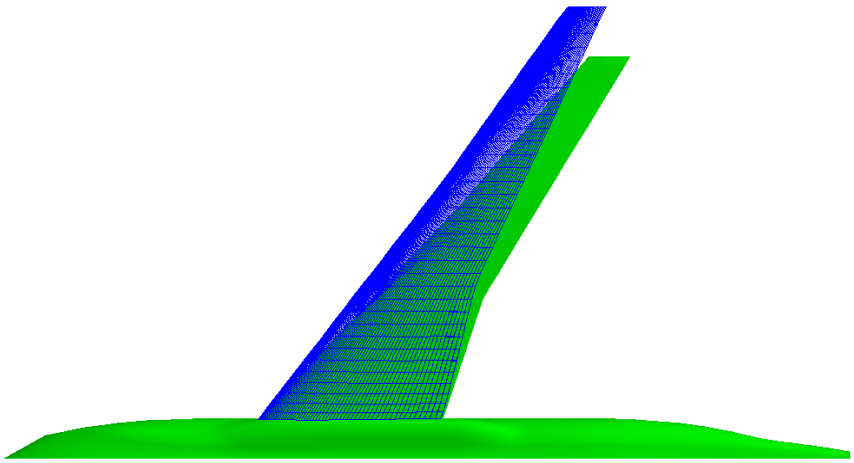

**Figure 7. Redesign of Boeing 747 planform using a single-point design method. The baseline (green) and the optimized section-and-planform (blue) geometries of Boeing 747 are over-plotted. The redesigned geometry has a longer span, a lower sweep angle, and thicker wing sections, improving both aerodynamic and structural performances. The optimization is performed at Mach .85 and fixed $C_L$ .45, where $\frac{\alpha_3}{\alpha_1}$ is chosen to maximize the range of the aircraft.**

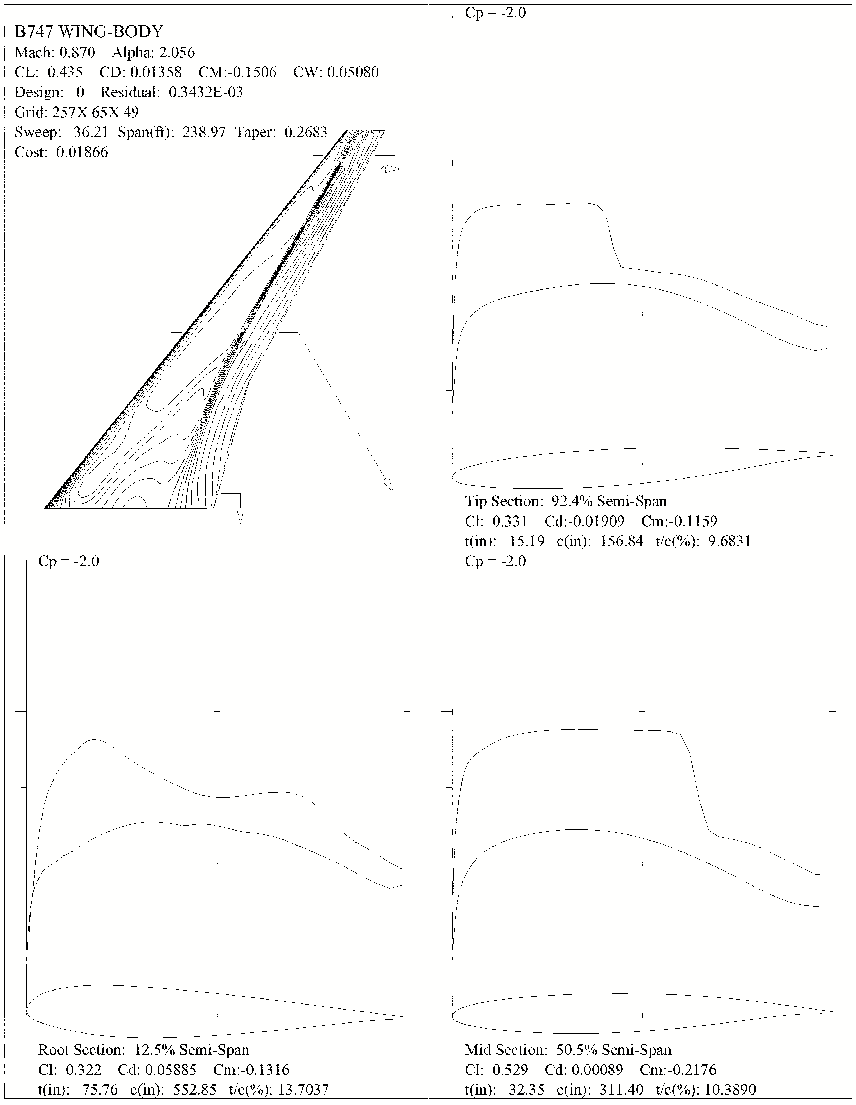


**Figure 8. Pressure Distribution on the Initial Geometry.**

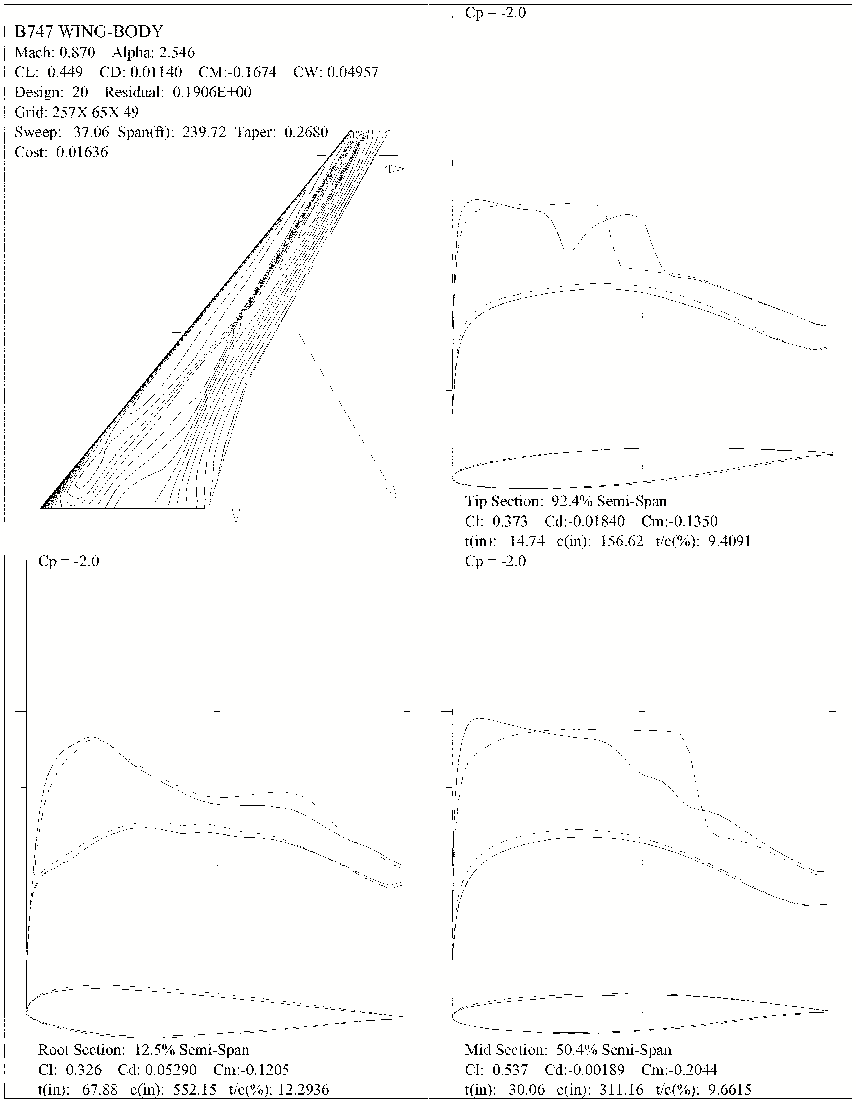


**Figure 9. Pressure Distribution on the Redesigned Geometry.**